# Asymmetric Brownian Motor Driven by Bubble Formation in a Hydrophobic Channel

**Noriyoshi Arai,[†,‡,§,*] Kenji Yasuoka,[‡] Takahiro Koishi,[⊥] and Toshikazu Ebisuzaki[§]**

[†]Department of Mechanical Engineering and Intelligent Systems, University of Electro-Communications, Chofu 182-8585, Japan, [‡]Department of Mechanical Engineering, Keio University, Yokohama 223-8522, Japan, [§]Computational Astrophysics Laboratory, RIKEN, Wako, Saitama 351-0198, Japan, and [⊥]Department of Applied Physics, University of Fukui, Bunkyo, Fukui 910-8507, Japan

**ABSTRACT** The "asymmetric Brownian ratchet model" is a variation of Feynman's ratchet and pawl system proposed. In this model, a system consisting of a motor and a rail has two binding states. One is the random Brownian state, and the other is the asymmetric potential state. When the system is alternatively switched between these states, the motor can be driven in one direction. This model is believed to explain nanomotor behavior in biological systems. The feasibility of the model has been demonstrated using electrical and magnetic forces; however, switching of these forces is unlikely to be found in biological systems. In this paper, we propose an original mechanism of transition between states by bubble formation in a nanosized channel surrounded by hydrophobic atoms. This amounts to a nanoscale motor system using bubble propulsion. The motor system consists of a hydrophobic motor and a rail on which hydrophobic patterns are printed. Potential asymmetry can be produced by using a left-right asymmetric pattern shape. Hydrophobic interactions are believed to play an important role in the binding of biomolecules and molecular recognition. The bubble formation is controlled by changing the width of the channel by an atomic distance (~0.1 nm). Therefore, the motor is potentially more efficient than systems controlled by other forces, in which a much larger change in the motor position is necessary. We have simulated the bubble-powered motor using dissipative particle dynamics and found behavior in good agreement with that of motor proteins. Energy efficiency is as high as 60%.

**KEYWORDS:** Brownian ratchet · molecular motor · bubble formation · dissipative particle dynamics · nanosized channel · hydrophobic pattern

Feynman proposed *the ratchet and pawl* system in 1963[1] to produce single direction motion from random thermal motions, using two heat reservoirs at different temperatures. This concept has since been modified by introducing Brownian particles in an asymmetric periodic potential to explain the working of nanosized motors in biological systems.[2−10] In this model, a motor particle and rail have two binding states: the random Brownian state and asymmetric potential state (see Figure 1). In the random Brownian state, the particle displays one-dimensional random walking movement along the rail. In the asymmetric potential state, the motor particle is subject to an asymmetric potential of sawtooth shape from the rail, in addition to random forces from ambient molecules. As the system alters state from Brownian to asymmetric and back, the motor particle stochastically moves in a single direction. The probability of forward movement is higher than reverse movement because of the asymmetric potential.[11] A similar idea was proposed for the actin−myosin system by Oosawa *et al.*[12−14]

Many researchers[3−9] have performed numerical simulations of this asymmetric Brownian motor, using assumptions about the interaction between the motor particle and rail. They revealed that it can work on a scale smaller than 100 nm, where thermal fluctuations are dominant. The energy efficiency of one motor system was estimated to be 0.02−0.05%[8] for the N-motor model, in which many (N-) motors are connected to each other. It could achieve an efficiency as high as 30−40%.[10] In numerical simulations, a motor particle moves in a stepwise manner corresponding to the length of the repeating structure on the rail which produces the asymmetric potential. While it can also move backward, the probability is much lower than the forward direction.

Similar behavior has been observed in the motion of a KIF1A molecule, the simplest biological motor protein, along a microtubule.[15,16] It showed stepwise motion of 8 nm units, which corresponded to the repeating pattern of the microtubule. The KIF1A molecule also showed a biased displacement when it bound with the microtubule.

The actin−myosin system produces muscle contraction and has been studied as a biological motor system.[17−20] Yanagida *et al.*[21] observed that the sliding movement of a single action filament per one ATP cycle

*Address correspondence to arai@mce.uec.ac.jp.

Received for review February 1, 2010 and accepted September 24, 2010.

**Published online October 5, 2010.**
**10.1021/nn101855d**

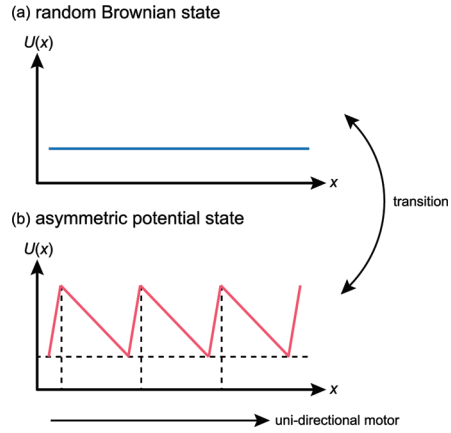


**Figure 1. Principle of the Brownian motor. The system of a motor particle and a rail has two states: (a) random Brownian state and (b) asymmetric potential state. As the system alternatively transits from (a) to (b) and back, the motor particle moves stochastically in one direction (to the right, in this case).**

was much greater than that of both the myosin head and actin molecule. However, the myosin molecule could also take a step backward during one ATP hydrolysis step. Thus, the myosin molecule fluctuated thermally and stochastically moved during ATP hydrolysis, which is called "loose coupling". This loose coupling behavior of the actin−myosin system is consistent with the asymmetric Brownian model and the concept proposed by Oosawa *et al.*[12−14] Asymmetric Brownian motors are useful for understanding the working principles of molecular motors in biological systems. They can explain the behavior of a simple motor protein such as KIF1A and also complex systems such as muscles.

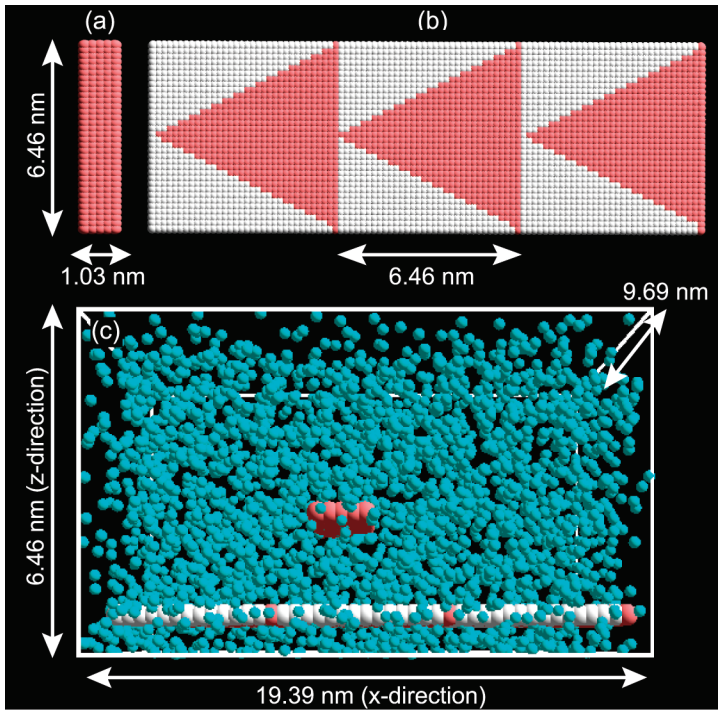


**Figure 2. Motor system composed of a motor and a rail. (a) Motor is a board made solely of strongly hydrophobic particles (red). (b) Rail is made of both strongly (red) and weakly (white) hydrophobic particles. The pattern of the strongly hydrophobic particle is left-right asymmetric, in this case using triangles. (c) Motor particle (red) and rail (red and white) are dipped in water.**

Researchers have carried out experiments for artificial Brownian motor systems, exploiting electric or magnetic fields as asymmetric potentials.[2,22−24] The size of the motor particle is submicrometer, and their efficiencies are as low as ∼8%. By nature of electrical and magnetic forces, motor particles in such systems inevitably move in directions regardless of the rail, making transitions between the two states (random Brownian state and asymmetric potential state).

In the present paper, we propose an alternative way to construct an asymmetric Brownian motor based on the hydrophobic (or equivalently capillary) interaction between two bodies immersed in water. Our model consists of a small board (a motor) with hydrophobic surfaces and a rail structure on which left-right asymmetric patterns of hydrophobic molecules are printed (see Figure 2). When the board is close to the rail, water molecules between them are expelled from the narrow channel. A bubble or vacuum then forms due to the higher potential between surrounding hydrophobic molecules.

The motor is pushed with a net force (capillary force) toward the rail. It is also subject to a net force in the horizontal direction because of the hydrophobic material pattern in the direction that maximizes the bubble area (the area surrounded by only hydrophobic molecules). Since the pattern on the rail is asymmetrically left-right oriented, the exerted force is naturally asymmetric. Switching of this hydrophobic interaction occurs based on the existence a single layer of water molecules. Therefore, our model can achieve a high efficiency with minimal (∼0.6 nm) change in position between the motor and rail. In practice, hydrophobic interactions between two biomolecules originate from similar bubble formation and a net attractive force. Such hydrophobic interactions are common in biomolecules including motor proteins.

We have performed numerical simulations using the dissipative particle dynamics (DPD) method and confirmed that an efficiency as high as 60% is attainable. DPD methods[25,26] allow us to perform simulations on a millisecond time scale and micrometer length scale since it simulates the motion of coarse-grained particles, which represents 10−20 atoms. In this study, we have performed calculations on behavior over several microseconds. It is not feasible to calculate on this time scale using molecular dynamics methods.

The following section explains the methodology in constructing a thermal ratchet model. We have achieved a thermal ratchet model by controlling bubble formation in the narrow channel between the motor and a rail. A comparison of this model to experimental data of a KIF1A motor protein is also given. We were able to achieve a higher efficiency when we placed another rail over the motor.

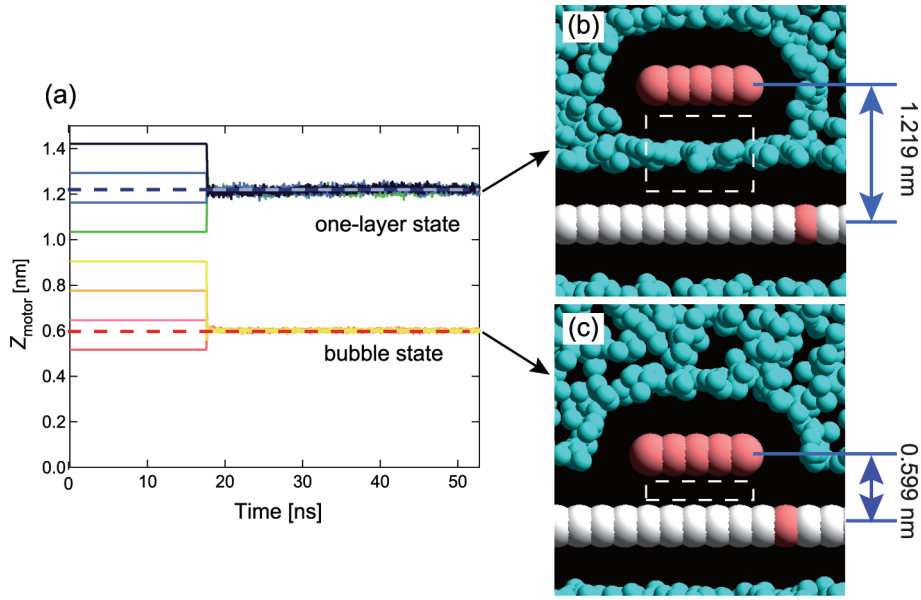


**Figure 3. (a) Time evolution of distance between the motor and the rail in the *z*-direction. The rail was located 0.646 nm in the *z*-direction. The dashed lines are the time average positions of the motor. (b,c) Snapshot of the side view around the motor; the distribution the water is projected to *x*−*z* plane, (c) *bubble state*, (b) *one-layer state*.**

Three particle types have been used in this study: strongly hydrophobic (labeled hs), weakly hydrophobic particles (labeled hw), and water particles (labeled w). The interactions between two particles are characterized by $a_{ij}$, where $a_{w\text{-}w} = a_{hw\text{-}hw} = a_{hs\text{-}hs} = 25\ k_BT$, $a_{w\text{-}hw} = a_{hw\text{-}hs} = 50\ k_BT$, and $a_{w\text{-}hs} = 100\ k_BT$. These hydrophilic and hydrophobic interactions are related to the solubility parameters.[27] Values for various materials have been examined by various research groups.[28−34] The interactions between the hydrophobic part and the water particle range from 50 to 130. Nearly half of the KIF1A and microtubule structures are hydrophobic amino acids, and parameters should be distributed among similar values. Thus, we have set these values to be constant for the model and believe that they are physically relevant values. The absolute values from this study have no specific meaning and will be further commented upon later. We adopted 100 and 50 $k_BT$ as the representative values for the two kinds of hydrophobicity, and the temperature was kept constant while the energy was normalized as $k_BT = 1$.

Koishi *et al.*[35,36] performed molecular dynamics simulations to study bubble formation in a narrow channel surrounded by a hydrophobic material and found that the phase transition in the confined nanochannel was different from that in the bulk.[37−39] Bubble formation exerted a net attractive force between the channel walls. They argued that this net attractive force was the origin of the hydrophobic interaction between two biomolecules. They also found that a force was also exerted in the horizontal direction to maximize the bubble area and to minimize total energy of the system.

On the basis of their results, we construct an asymmetric Brownian motor as follows (Figure 2). A rail and a motor molecule are embedded in water. The motor is made solely of strongly hydrophobic particles (red). The rail is made of both strongly (red) and weakly (white) hydrophobic particles. The pattern of the strongly hydrophobic particles is left-right asymmetric. The *x*-, *y*-, and *z*-directions were taken to be along the asymmetric pattern of the rail, across the asymmetric pattern of the rail, and perpendicular to the rail surface, respectively.

We assume the rail and motor to be rigid: the particles in the motor and the rail do not move with respect to the centers of mass. We take the center of mass of the rail as the coordinate origin.

$$\mathbf{R}_{rail} = (0, 0, 0) \tag{1}$$

The position of the motor is calculated by

$$M\frac{d^2X_{motor}}{dt^2} = F_x/N_m \tag{2}$$

$$M\frac{d^2Y_{motor}}{dt^2} = 0,\ Y_{motor} = 0 \tag{3}$$

$$M\frac{d^2Z_{motor}}{dt^2} = F_z/N_m \tag{4}$$

where $F_x = \sum_i^{N_m} f_{x,i}$ and $F_z = \sum_i^{N_m} f_{z,i}$, $M$, $X_{motor}$, $Y_{motor}$, and $Z_{motor}$ are the mass and position of the motor in *x*-, *y*-, *z*-directions, $N_m$ is the number of particles that composes the motor. The motor only moves in *x*- and *z*-directions, and rotation may also occur.

**TABLE 1. Result for Simulation of Natural Binding State**

| case | $z_0$ (nm) | average from 44.0 to 52.8 ns (nm) |
|---|---|---|
| 1 | 0.517 | 0.599 |
| 2 | 0.646 | 0.599 |
| 3 | 0.776 | 0.600 |
| 4 | 0.905 | 0.600 |
| 5 | 1.034 | 1.213 |
| 6 | 1.163 | 1.222 |
| 7 | 1.293 | 1.221 |
| 8 | 1.422 | 1.220 |

The cutoff radius of the DPD parameter, $r_c$, is 0.646 nm. We have adopted the method by Groot and Rabone for sealing of length and time.[27] We used 17 070 particles in total. The number of water, rail, and motor particles was 13 500, 3400, and 170, respectively. The simulation box size was 19.39 × 9.69 × 6.46 nm$^3$, and we used periodic boundary conditions.

## RESULTS AND DISCUSSION

The motion of the motor without any external force was observed to study the natural binding states of the system. The simulation was started from various initial conditions, where $Z_{motor} = Z_0$, and $Z_0$ was set at 0.517, 0.646, 0.776, 0.905, 1.034, 1.163, 1.293, and 1.422 nm. The position of the motor was first restricted to $Z_{motor} = Z_0$ for 17.6 ns to equilibrate the distribution of the water molecules. The position was allowed to subsequently move in the $z$-direction to investigate the change in $Z_{motor}$, as shown in Figure 3. For the cases of $Z_0$ = 1.034, 1.163, 1.293, and 1.422 nm, the $Z_{motor}$ converged to $z \sim 1.219$ nm, and a *one-layer state* of water molecules was formed between the motor and rail (Figure 3b). On the contrary, for cases of $Z_0$ = 0.517, 0.646, 0.776, and 0.905 nm, the motor position converged into $z \sim 0.599$ nm (Table 1). In such cases, no water particles were located in the channel between the motor and rail, as can be seen in Figure 3c. This state is named the *bubble state*, and this observation suggests that the system has two distinct binding states.

The time averaged force $\langle F_x \rangle$ exerted on the motor from the water particles for these two states was calculated. The time averaged force $\langle F_x \rangle$ is negligible for all positions in the one-layer state (blue dots in Figure 4a). A finite net force exists in the bubble state because the distribution of ambient particles around the motor is not symmetric, due to the hydrophobic pattern printed on the rail surface (red dots in Figure 4a). The shape of the net force on the motor particle corresponds to the asymmetric potential shown in Figure 1; in other words, the bubble state corresponds to the asymmetric potential state, and the one-layer state corresponds to the random Brownian state for the asymmetric Brownian motor model.

The contour curves for the density of water particles around the motor are shown in Figure 4b,c for $X_{motor} = 4.28$. In the case of the bubble state, a high density region is located around the motor. The length of the high density region in the left-hand side is greater than that in the right-hand side because of the asymmetry of the hydrophobic patterns on the rail. The bias

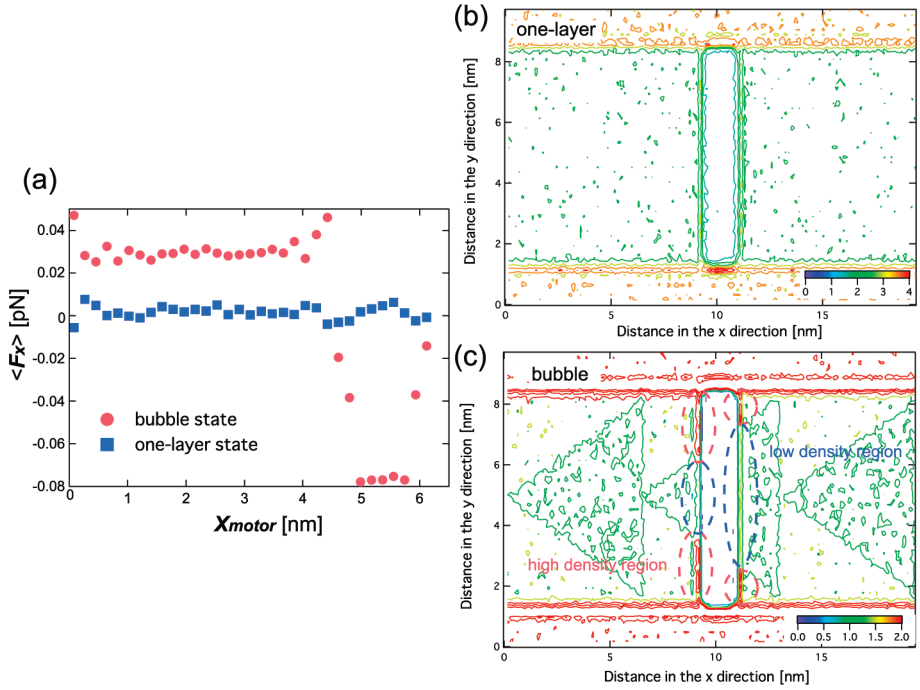


**Figure 4. (a) Time average force acting on the motor $\langle F_x \rangle$ in the $x$-direction. The horizontal axis is the position of the motor and shows one periodic pattern of the rail. The blue points and red points are $z \sim 1.219$ nm (one-layer state) and $z \sim 0.599$ nm (bubble state), respectively. (b) Contour line of water density around the motor $z = 1.219$ nm (one-layer state). (c) Same as for (b) but with $z = 0.599$ nm (bubble state). As can be seen in (a), the one-layer state and bubble state correspond to the random Brownian state and asymmetric potential state, respectively.**

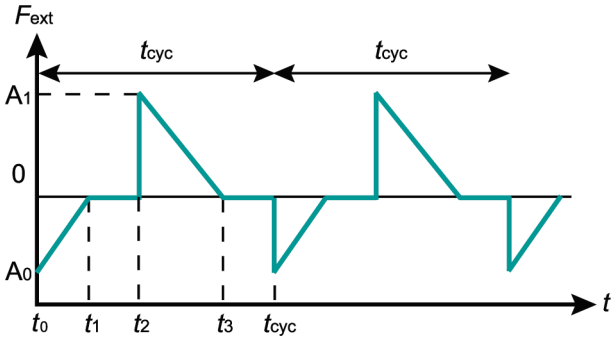


**Figure 5. External force, $F_{ext}$, acting on the motor particle in the one-layer state in the *z*-direction during the period of $t_{cyc}$. The time sequence is divided into four phases: (1) $t_0 - t_1$, the motor particle is pushed downward to the rail transit to the bubble state; (2) $t_1 - t_2$, no external force is applied; (3) $t_2 - t_3$, the motor particle is pushed upward from the rail to cause the bubble to vanish (transit to one-layer state); (4) $t_3 - t_{cyc}$, no external force is applied.**

of high density regions causes the net force. In contrast, in the one-layer state (Figure 4b), there is no clear density enhancement around the motor, which corresponds to the net force exerted on the motor being almost zero.

The alternating between the one-layer state and the bubble state was accomplished by applying an external force to the motor molecule in the *z*-direction, as shown in Figure 5.

The procedure of applying the external force is as follows. The external force acts on the motor molecule from $t_0$ to $t_1$, and the system shifts from the bubble to one-layer state (Figure 6); $F_{ext}$ is kept at zero from $t_1$ to $t_2$. Subsequently, from $t_2$ to $t_3$, the external force acts downward on the motor to give a transition from the one-layer to the bubble states. From $t_3$ to $t_{cyc}$, the external force is kept at zero again, and this pattern of force exerted is repeated for a period of $t_{cyc}$.

We optimized the values of $A_1$, $A_0$, $t_1$, $t_2$, $t_3$, and $t_{cyc}$ for driving the motor system. The parameter $A_0$ is the magnitude of the external force for conversion from the one-layer state to the bubble state, and $A_1$ is the magnitude of the external force for the opposite conversion from the bubble state to the one-layer state. If the external force is too strong, the motor moves too far from the rail, considerably decreasing the efficiency because of unnecessary work. If the external force is too weak, the motor does not show a transition between the two states. For time parameters ($t_0$, $t_1$, $t_2$, $t_3$, and $t_{cyc}$), we chose the values in which the motor molecule sufficiently diffused with a short computing time. The parameters in Figure 5 are shown in Table 2.

Figure 6 shows the time evolution of $X_{motor}$ and $Z_{motor}$. The probability for the positive *x*-direction is higher than that for the negative *x*-direction. Thus, the motor moves forward, though there is no net force. The motor motion is stochastic for the x-direction, during the bubble layer state as shown in the figure inset.

The motor moves randomly in the one-layer state, corresponding to the random Brownian motion state. The motor stochastically moved in one direction, and the asymmetric Brownian model is achieved in this system. The motor molecule moved stepwise with a step factor of 6.46 nm, and this step size corresponds to the period of the triangle pattern of the rail. The motor in this study moves up and down in the *z*-direction due to an external force. The behavior seen in Figure 6 is similar to the motor protein, KIF1A.[16,40]

We measured deviations of the $X_{motor}$ in the one-layer state and the bubble state (Figure 7). In the one-layer state, the distribution of the displacement of

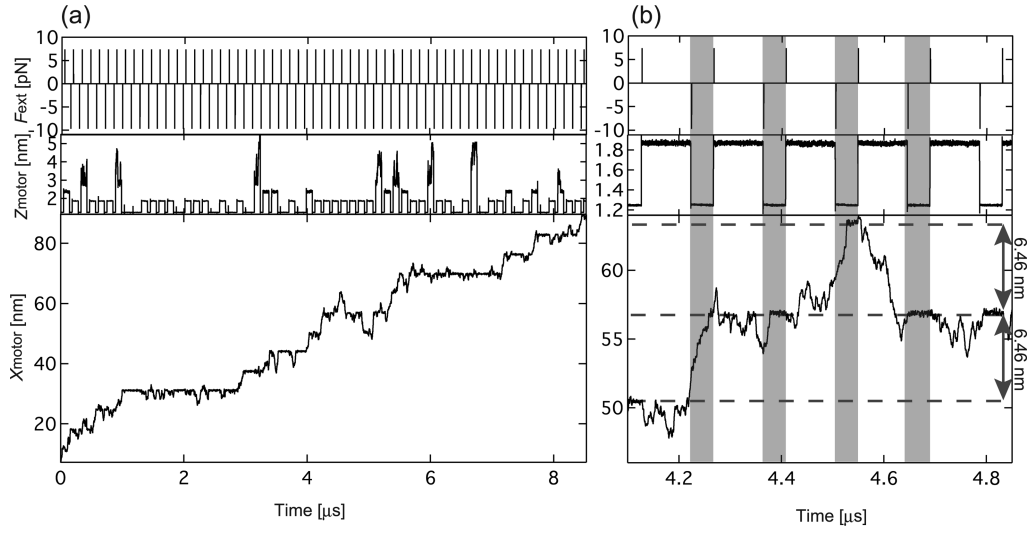


**Figure 6. (a) External force, $F_{ext}$; the coordinate of the motor, $X_{motor}$, $Z_{motor}$, as the function of time. (b) Close-up view from 4.1 to 4.85 μs. The gray area represents the bubble state. One direction motion is invoked in the bubble state because of the asymmetric potential.**

**TABLE 2. Parameters for the External Force**

| $A_0$ (pN) | $A_1$ (pN) | $t_1$ (ns) | $t_2$ (ns) | $t_3$ (ns) | $t_{cyc}$ (ns) |
|---|---|---|---|---|---|
| −9.73 | 7.49 | 0.35 | 43.99 | 44.20 | 140.78 |

$X_{motor}$ is similar to the Gaussian distribution. The movement of the motor in the one-layer state is a single direction Brownian motion. The motor hardly moves in the *x*-direction of the bubble state because it is captured with a potential pocket.

The energy efficiency, η, of the motor system can be estimated by the work in the *x*-direction required to move surrounding water molecules, divided by that done by the external force in the *z*-direction:

$$\eta = \frac{\Delta t \sum_{t_s}^{t_t} \left( \sum_{i}^{N_m} F_{x,i} \right)(x_k - x_{k-1})}{\Delta t \sum_{t_s}^{t_t} F_{ext}(z_k - z_{k-1})} \quad (5)$$

where $t_s$ and $t_t$ are the start and termination times of the measurement, respectively, and $F_{x,i}$ is the conservation force exerted by the *i*-th particle composing the motor; $x_k$ and $z_k$ are the positions at the *k*-th time step, and $\Delta t$ is the time step. The efficiency was about 39% for an average of four simulations. We also examined the efficiency of other physical conditions (temperatures and hydrophobic interaction parameters).

We carried out calculations over a temperature range of 0.90 to 1.10 with increments of 0.05. As a result, efficiencies in $T = 0.90$, 0.95, 1.05, and 1.10 $k_BT$ were about 20, 26, 43, and 47%, respectively.

The movement of the water molecule becomes slow when the temperature is low, and the phase transition does not occur easily, hence a lower efficiency. Conversely, the water molecule moves more actively when the temperature is higher, and phase transition occurs more easily. Hence, efficiency is higher. When the temperature is increased further than earlier, the attraction between the motor and rail becomes relatively weak and the efficiency decreases.

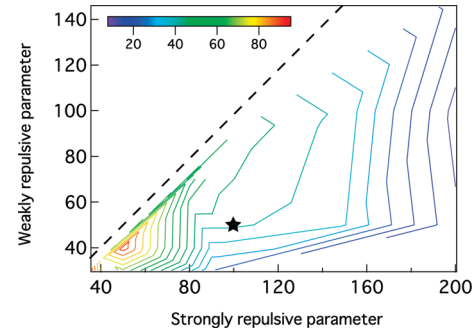


**Figure 8. Contour line of efficiency in our model. Dashed line indicates that a strongly repulsive parameter ($a_{w\text{-}hs}$) and a weakly repulsive parameter ($a_{w\text{-}hw}$, $a_{hw\text{-}hs}$) are the same. The condition discussed is denoted by a star.**

An exploration on the hydrophobic interaction parameter $a_{ij}$ was also performed. A strong parameter is changed from 35 to 200, and a weak parameter is changed from 30 to 150 (see Figure 8). A bubble is formed easily and is not broken when the difference between strong and weak parameters is large. On the contrary, a bubble is broken easily and is not formed when the difference between strong and weak parameters is small. Similarly, the water and hydrophobic interaction parameters also affect the efficiency in this model. A bubble is formed easily and is not broken when the difference between water and hydrophobic interaction parameters is large. On the contrary, a bubble is broken easily and is not formed when the difference between water and hydrophobic interaction parameters is small. In this model, when the strong and weak hydrophobic parameters are 50 and 40 $k_BT$, respectively, the model motor efficiency is at its highest. Consequently, the essence of the proposed mechanism is that there are two kinds of hydrophobicity but no physical meaning of a specific value.

As can be seen in Figure 6, a considerable amount of work is lost by (1) abrupt increases in $Z_{motor}$ beyond the one-layer state and (2) backward motion. Such unnecessary motor motions are prohibited in a double-sided motor. In this system, we placed another rail over

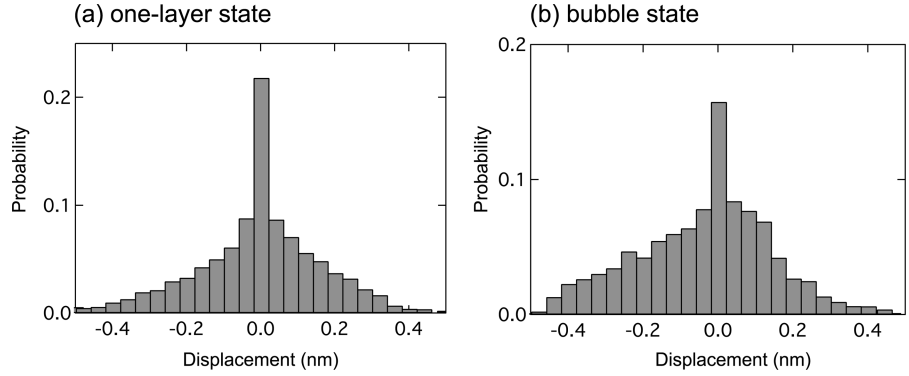


**Figure 7. Deviations of the $X_{motor}$ in one step. The deviation is left-right symmetric in the one-layer state (a) but asymmetric in the bubble state (b).**

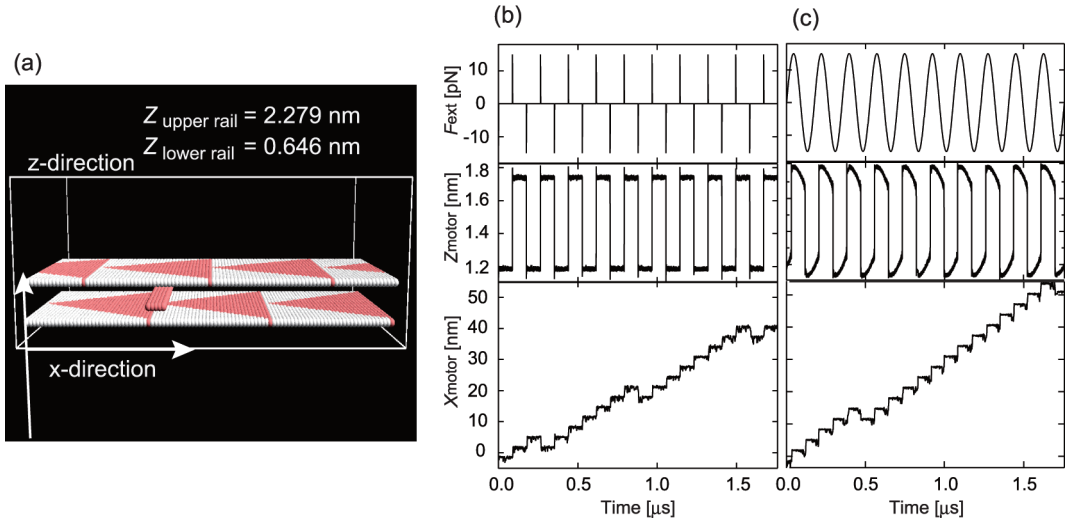


**Figure 9. (a) Double-sided motor system. Water particles are not shown. (b) Same as Figure 6b but for the double-sided motor system. (c) External force form is changed from Figure 5 to a sine wave ($F_{ext} = A \sin(2\pi/t_{cyc})$, $A = 14.97$ pN, $t_{cyc} = 175.975$ ns).**

the motor molecule, as shown in Figure 9. The asymmetric patterns are shifted by a half of the periodicity. The sizes of the rail and motor are the same in the earlier simulations, and the external force for the phase transition is given in Table 3. It was designed so that, when the motor proceeds closer to the lower rail, the distance between the lower rail and motor is in the range of the bubble state, and the distance between the upper rail and motor is in the range of the one-layer state. The opposite applies when the motor gets closer to the upper rail. Finally, simulations where the external force is switched from that of Figure 5 to a sine wave were carried out (Figure 9c). It was possible to move the motor in a similar manner to the earlier simulations. The efficiency was 41%.

Host−guest bindings due to the hydrophobic interaction are common in biological systems, such as the KIF1A/microtubule system. The behavior of the motor shown in Figure 6 is remarkably similar to that of KIF1A, investigated by other research groups.[15,16,40] Okada *et al.*[15,16] measured the movement behavior of a KIF1A and found two characteristic binding states, a *strong binding state* and a *weak binding state*, during the ATP hydrolysis process. In the strong binding state, KIF1A is tightly bound to a specific site of the microtubule. In the other state, KIF1A is loosely bound to the microtubule, and KIF1A shows a one-dimensional random motor microtubule. The transition from a tight binding to weak binding state takes place at the expense of the chemical release of energy during ATP hydrolysis. The switch between these two states is achieved by molecular conformational change.

**TABLE 3. Parameters about the External Force for the Double-Sided Motor System**

| $A_0$ (pN) | $A_1$ (pN) | $t_1$ (ns) | $t_2$ (ns) | $t_3$ (ns) | $t_{cyc}$ (ns) |
|---|---|---|---|---|---|
| −14.97 | 14.97 | 1.76 | 87.99 | 89.74 | 175.97 |

In our study, the motor moves up and down due to an external force, and it models the conformational change during ATP hydrolysis. The external force corresponds to chemical energy that is acquired by this cycle. The bubble and one-layer states correspond to strong and weak binding states, respectively.

This study has demonstrated a nanomotor system using bubble propulsion, which is a new mechanism. It has been compared with other artificial Brownian motor systems that use electric or magnetic fields as an asymmetric potential.[2,23] Rousselet *et al.*'s ratchet system[2] controlled the motion of colloidal particles using a sawtooth dielectric potential field. The field was generated by an interdigitated electrode deposited on a glass slide, which had a Christmas tree structure. The size of the patterns and particles was about 50 and 0.25 μm, respectively. Villegas *et al.*[23] demonstrated the ratchet system with superconducting critical temperatures between 8.3 and 8.7 K using a magnetic field. It stands to reason that the motor actually moved according to Feynman's ratchet model in our system. The advantage of our motor system is that it can be integrated because of its reduced size (nanometer order).

The alternating reaction is distinct and easy to control because it uses the bubble nucleation phenomenon (the motor stays at the targeted position $z \sim 0.599$ and 1.219 nm in this model). This mechanism only needs to control the gap between the motor and rail, so high efficiency is expected.

## CONCLUSION

Our molecular simulation showed that the "asymmetric Brownian ratchet model" can be achieved by a

system with a motor and a rail which has asymmetric hydrophobic patterns. The mechanism uses bubble propulsion: the phase transition between the bubble and one-layer states acts as a switch. The switching time is as short as 50 ns. This mechanism needs only to the control the gap between the motor and rail by one molecule length (about 5−6 Å). The behavior of the motor molecule obtained in this model is similar to that of the KIF1A motor protein.

Our motor system is small enough to accumulate it like a integrated circuit. It is applicable to machine elements which are required to operate continuously.

## METHOD

The DPD method uses Newton's equation of motion for a particle *i*,

$$m_i \frac{d\mathbf{v}_i}{dt} = \mathbf{f}_i = \sum_{j \neq i} \mathbf{F}_{ij}^{C} + \sum_{j \neq i} \mathbf{F}_{ij}^{D} + \sum_{j \neq i} \mathbf{F}_{ij}^{R} \quad (6)$$

where $m$ is the mass, $\mathbf{v}$ the velocity, $\mathbf{F}_{ij}^{C}$ the conservative force, $\mathbf{F}_{ij}^{R}$ the pairwize random force, and $\mathbf{F}_{ij}^{D}$ the dissipative force. The conservative force is softly repulsive and is given by

$$\mathbf{F}_{ij}^{C} = \begin{cases} -a_{ij}\left(1 - \frac{|\mathbf{r}_{ij}|}{r_c}\right)\mathbf{n}_{ij}, & |\mathbf{r}_{ij}| \leq r_c \\ 0, & |\mathbf{r}_{ij}| > r_c \end{cases} \quad (7)$$

where $\mathbf{r}_{ij} = \mathbf{r}_j - \mathbf{r}_i$, and $\mathbf{n}_{ij} = \mathbf{r}_{ij}/|\mathbf{r}_{ij}|$. Here, $a_{ij}$ is a parameter to determine the magnitude of the repulsive force between particles *i* and *j*, and $r_c$ is the cutoff distance. Random force ($\mathbf{F}_{ij}^{R}$) and dissipative force ($\mathbf{F}_{ij}^{D}$) are given by

$$\mathbf{F}_{ij}^{R} = \begin{cases} \sigma\omega^{R}(|\mathbf{r}_{ij}|)\zeta_{ij}\Delta t^{-1/2}\mathbf{n}_{ij}, & |\mathbf{r}_{ij}| \leq r_c \\ 0, & |\mathbf{r}_{ij}| > r_c \end{cases} \quad (8)$$

and

$$\mathbf{F}_{ij}^{D} = \begin{cases} -\gamma\omega^{D}(|\mathbf{r}_{ij}|)(\mathbf{n}_{ij}\cdot\mathbf{v}_{ij})\mathbf{n}_{ij}, & |\mathbf{r}_{ij}| \leq r_c \\ 0, & |\mathbf{r}_{ij}| > r_c \end{cases} \quad (9)$$

where $\mathbf{v}_{ij} = \mathbf{v}_j - \mathbf{v}_i$, $\sigma$ is the noise parameter, $\gamma$ the friction parameter, and $\zeta_{ij}$ the random number based on the Gaussian distribution. Here $\omega^R$ and $\omega^D$ are *r*-dependent weight functions which are given by

$$\omega^{D}(r) = [\omega^{R}(r)]^2 = \begin{cases} 1 - \frac{|\mathbf{r}_{ij}|}{r_c}, & r_{ij} \leq r_c \\ 0, & r_{ij} > r_c \end{cases} \quad (10)$$

The temperature is controlled by a combination of dissipative and random forces. The noise parameter $\sigma$ and friction parameter $\gamma$ are connected to each other by the fluctuation−dissipation theorem in the following equation

$$\sigma^2 = 2\gamma k_B T \quad (11)$$

where $k_B$ is the Boltzmann constant and $T$ is the temperature.

*Acknowledgment.* The simulation study was supported by the Core Research for Evolution Science and Technology (CREST) of the Japan Science and Technology Corporation (JST), and a Grant-in-Aid for the Global Center of Excellence Program for the "Center for Education and Research of Symbiotic, Safe and Secure System Design" from the Ministry of Education, Culture, Sport, and Technology in Japan.

*Supporting Information Available:* Movie 1: the motor motion in nanoscale motor system using bubble propulsion. The bubble formation is controlled by changing the width of the channel between a motor and a rail by an atomic distance. Water particles just inside the channel are displayed. The bubble state in the channel corresponds to the asymmetric potential state, and the one-layer state in the channel corresponds to the random Brownian state for Feynman's asymmetric Brownian motor model. Movie 2: the motor motion in double-sided motor. In this system, we placed another rail over the motor molecule. The asymmetric patterns are shifted by a half of the periodicity. The external force for the phase transition is given in a sine wave. It was designed so that when the motor proceeds closer to the lower rail, the distance between the lower rail and motor is in the range of the bubble state, and the distance between the upper rail and motor is in the range of the one-layer state. The opposite applies when the motor gets closer to the upper rail. Water particles just inside the channels are displayed. This material is available free of charge *via* the Internet at http://pubs.acs.org.

## REFERENCES AND NOTES

1. Feynman, R. P.; Leighton, R. B.; Sands, M. *Feynman Lectures on Physics*; Addison-Wesley: Reading, MA, 1963; Vol. 1; Chapter 46.
2. Rousselet, J.; Salome, L.; Ajdari, A.; Prost, J. Directional Motion of Brownian Particles Induced by a Periodic Asymmetric Potential. *Nature* **1994**, *370*, 446–448.
3. Córdova, N. J.; Ermentrout, B.; Oster, G. F. Dynamics of Single-Motor Molecules: The Thermal Ratchet Model. *Proc. Natl. Acad. Sci. U.S.A.* **1992**, *89*, 339–343.
4. Magnasco, M. O. Forced Thermal Ratchets. *Phys. Rev. Lett.* **1993**, *71*, 1477–1481.
5. Doering, C. R.; Horsthemke, W.; Riordan, J. Nonequilibrium Fluctuation-Induced Transport. *Phys. Rev. Lett.* **1994**, *72*, 2984–2987.
6. Astumian, R. D.; Bier, M. Fluctuation Driven Ratchets: Molecular Motors. *Phys. Rev. Lett.* **1994**, *72*, 1766–1769.
7. Prost, J.; Chauwin, J.-F.; Peliti, L.; Ajdari, A. Asymmetric Pumping of Particles. *Phys. Rev. Lett.* **1994**, *72*, 2652–2655.
8. Sekimoto, K. Kinetic Characterization of Heat Bath and the Energetics of Thermal Ratchet Models. *J. Phys. Soc. Jpn.* **1997**, *66*, 1234–1237.
9. Jülicher, F.; Ajdari, A.; Prost, J. Modeling Molecular Motors. *Rev. Mod. Phys.* **1997**, *69*, 1269–1281.
10. Mouri, K.; Shimokawa, T. Effect of the Number of Molecules on the Energetic Efficiency in Molecular Motors Using the Flashing Ratchet Model. *Physica A* **2008**, *387*, 5169–5181.
11. Astumian, R. D. Making Molecules into Motors. *Sci. Am.* **2001**, *285*, 56–64.
12. Oosawa, F.; Masai, J. Mechanism of Flagellar Motor Rotation in Bacteria. *J. Phys. Soc. Jpn.* **1982**, *51*, 631–641.
13. Oosawa, F.; Hayashi, S. Coupling between Flagellar Motor Rotation and Proton Flux in Bacteria. *J. Phys. Soc. Jpn.* **1983**, *52*, 4019–4028.
14. Oosawa, F.; Hayashi, S. The Loose Coupling Mechanism in Molecular Machines of Living Cells. *Adv. Biophys.* **1986**, *22*, 151–183.
15. Okada, Y.; Hirokawa, N. A Processive Single-Headed Motor: Kinesin Superfamily Protein KIF1A. *Science* **1999**, *283*, 1152–1157.
16. Okada, Y.; Higuchi, H.; Hirokawa, N. Processivity of the Single-Headed Kinesin KIF1A through Biased Binding to Tubulin. *Nature* **2003**, *424*, 574–577.
17. Huxley, A. F. Muscle Structure and Theories of Contraction. *Prog. Biophys. Biophys. Chem.* **1957**, *7*, 255–318.
18. Huxley, H. E. The Mechanism of Muscular Contraction. *Science* **1969**, *164*, 1356–1365.
19. Huxley, A. F.; Simmons, R. M. Proposed Mechanism of Force Generation in Striated Muscle. *Nature* **1971**, *233*, 533–538.

20. Vale, R. D.; Oosawa, F. Protein Motors and Maxwell's Demons: Does Mechanochemical Transduction Involve a Thermal Ratchet? *Adv. Biophys.* **1990**, *26*, 97–134.
21. Yanagida, T.; Arata, T.; Oosawa, F. Sliding Distance of Actin Filament Induced by a Myosin Crossbridge during One ATP Hydrolysis Cycle. *Nature* **1985**, *316*, 366–369.
22. Tsong, T. Y.; Xie, T. D. Ion Pump as Molecular Ratchet and Effects of Noise: Electric Activation of Action Pumping by Na, K-ATPase. *Appl. Phys. A: Mater. Sci. Process.* **2002**, *75*, 345–352.
23. Villegas, J. E.; Savel'ev, S.; Nori, F.; Gonzalez, E. M.; Anguita, J. V.; Garcia, R.; Vicent, J. L. A Superconducting Reversible Rectifier That Controls the Motion of Magnetic Flux Quanta. *Science* **2003**, *302*, 1188–1191.
24. Hänggi, P.; Marchesoni, F. Artificial Brownian Motors: Controlling Transport on the Nanoscale. *Rev. Mod. Phys.* **2009**, *81*, 387–442.
25. Hoogerbrugge, P. J.; Koelman, J. M. V. A. Simulating Microscopic Hydrodynamic Phenomena with Dissipative Particle Dynamics. *Europhys. Lett.* **1992**, *19*, 155–160.
26. Groot, R. D.; Warren, P. B. Dissipative Particle Dynamics: Bridging the Gap between Atomistic and Mesoscopic Simulation. *J. Chem. Phys.* **1997**, *107*, 4423–4435.
27. Groot, R. D.; Rabone, K. L. Mesoscopic Simulation of Cell Membrane Damage, Morphology Change and Rupture by Nonionic Surfactants. *Biophys. J.* **2001**, *81*, 725–736.
28. Ryjkina, E.; Kuhn, H.; Rehage, H.; Müller, F.; Peggau, J. Molecular Dynamic Computer Simulations of Phase Behavior of Non-ionic Surfactants. *Angew. Chem., Int. Ed.* **2002**, *41*, 7115–7119.
29. Shillcock, J. C.; Lipowsky, R. Equilibrium Structure and Lateral Stress Distribution of Amphiphilic Bilayers from Dissipative Particle Dynamics Simulations. *J. Chem. Phys.* **2002**, *117*, 5048–5061.
30. Shillcock, J. C.; Lipowsky, R. Exploring Vesicle Fusion with Dissipative Particle Dynamics. *Nat. Mater.* **2005**, *4*, 225–228.
31. Nakamura, H.; Tamura, Y. Phase Diagram for Self-Assembly of Amphiphilic Molecule C12E6 by Dissipative Particle Dynamics Simulation. *Comput. Phys. Commun.* **2005**, *169*, 139–143.
32. Yamamoto, S.; Hyodo, S. Mesoscopic Simulation of the Crossing Dynamics at an Entanglement Point of Surfactant Threadlike Micelles. *J. Chem. Phys.* **2005**, *122*, 204907.
33. Özen, A. S.; Sen, U.; Atilgan, C. Complete Mapping of the Morphologies of Some Linear and Graft Fluorinated Co-oligomers in an Aprotic Solvent by Dissipative Particle Dynamics. *J. Chem. Phys.* **2006**, *124*, 064905.
34. Illya, G.; Lipowsky, R.; Shillcock, J. C. Two-Component Membrane Material Properties and Domain Formation from Dissipative Particle Dynamics. *J. Chem. Phys.* **2006**, *125*, 114710.
35. Koishi, T.; Yoo, S.; Yasuoka, K.; Zeng, X. C.; Narumi, T.; Susukita, R.; Kawai, A.; Furusawa, H.; Suenaga, A.; Okimoto, N.; *et al.* Nanoscale Hydrophobic Interaction and Nanobubble Nucleation. *Phys. Rev. Lett.* **2004**, *93*, 185701.
36. Koishi, T.; Yasuoka, K.; Ebisuzaki, T.; Yoo, S.; Zeng, X. C. Large-Scale Molecular-Dynamics Simulation of Nanoscale Hydrophobic Interaction and Nanobubble Formation. *J. Chem. Phys.* **2005**, *123*, 204707.
37. Koga, K.; Gao, G. T.; Tanaka, H.; Zeng, X. C. Formation of Ordered Ice Nanotubes inside Carbon Nanotubes. *Nature* **2001**, *412*, 802–805.
38. Bai, J.; Wang, J.; Zeng, X. C. Multiwalled Ice Helixes and Ice Nanotubes. *Proc. Natl. Acad. Sci. U.S.A.* **2006**, 19664–19667.
39. Arai, N.; Yasuoka, K.; Zeng, X. C. Self-Assembly of Surfactants and Polymorphic Transition in Nanotubes. *J. Am. Chem. Soc.* **2008**, *130*, 7916–7920.
40. Tomishige, M.; Klopfenstein, D. R.; Vale, R. D. Conversion of Unc104/KIF1A Kinesin into a Processive Motor after Dimerization. *Science* **2002**, *297*, 2263–2267.